arXiv:1504.06007v1 [cond-mat.quant-gas] 22 Apr 2015

Universal characterizing topological insulator and topological semi-metal with Wannier functions

Ye Xiong
Department of Physics and Institute of Theoretical Physics ,
Nanjing Normal University, Nanjing 210023, P. R. China[*]

Peiqing Tong
Department of Physics and Institute of Theoretical Physics ,
Nanjing Normal University, Nanjing 210023, P. R. China[*]
Jiangsu Key Laboratory for Numerical Simulation of Large Scale Complex Systems,
Nanjing Normal University, Nanjing 210023, P. R. China and
Kavli Institute for Theoretical Physics China, CAS, Beijing 100190, China[†]

The nontrivial evolution of Wannier functions (WF) for the occupied bands is a good starting point to understand topological insulator. By modifying the definition of WFs from the eigenstates of the projected position operator to those of the projected modular position operator, we are able to extend the usage of WFs to Weyl metal where the WFs in the old definition fails because of the lack of band gap at the Fermi energy. This extension helps us to universally understand topological insulator and topological semi-metal in a same framework. Another advantage of using the modular position operators in the definition is that the higher dimensional WFs for the occupied bands can be easily obtained. We show one of their applications by schematically explaining why the winding numbers $\nu_{3D} = \nu_{2D}$ for the 3D topological insulators of DIII class presented in Phys. Rev. Lett. 114, 016801(2015).

PACS numbers: 73.43.-f, 03.65.Vf, 71.20.Nr, 71.10.Ca

I. INTRODUCTION

The discovery of quantum Hall effect [1], for the first time, sheds light on the topological properties of electronic bands hidden behind the 2-dimensional (2D) Fermi gas in magnetic field. Thouless *et al.* (referred as TKNN) calculated the Hall conductance by Kubo formula [2] and expressed it as an integral in the whole first Brillouin zone (FBZ). Then Simon *et al.* recognized the integral as the first Chern class of the U(1) principal fiber bundle on the torus of the FBZ [3–5]. Besides this route, Laughlin raised another way to understand quantum Hall effect by a gauge invariant argument (referred as the Laughlin argument on a cylinder) [6]. These two ways are equivalent but the latter one is more profound in explaining the robustness of the Hall conductance against local disorders because it is based on the global gauge arguments of the 2D electron system.

For topological insulators (TI), e. g., 2D spin Hall system [7] and 3D strong or weak TI [8–10], there are also two routes, parallel to those for quantum Hall effect, to understand their topological properties. One is the topological invariant, likes the Hall conductance in the TKNN theorem, that can be expressed as an integral in a portion of the FBZ [9–14]. The other route, similar to the Laughlin argument, is based on the evolution of the Wannier centers (WC) of the localized Wannier functions (WF) (along one direction) as a function of the momentum (in the perpendicular directions). These two routes are also equivalent. For instance, in Ref. [7], the Z_2 topological invariant in the 2D spin Hall system is defined by the switch partners of the WFs, which can be schematically illustrated by the evolution of WCs in the x direction as a function of momentum in the y direction, k_y. In Ref. [15–17], the topological invariant for 2D and 3D TIs are also associated with the evolution of the WCs as a function of k_y (and k_z) as well. Beside the schematic illustration of the nontrivial topological bands, WFs are also a good one-particle basis to study the many-body wave functions of the fractional topological insulator by mimicking the combination of these WFs as that of the Landau orbitals playing roles in the Laughlin state in the fractional quantum Hall effect [18, 19], or introducing pump process to axion coupling directly. [20]

Besides TI, another group of topological materials, called topological semi-metal (TM), such as Weyl metal, has attracted great interest for their exotic surface states and bulk behaviors in recent years[21–23]. Weyl metal does not have topological invariant defined in the 3D FBZ because bands touch at the Weyl points so that there is no band gap separating the occupied and the empty bands. One usually needs to split the 3D FBZ into a series of 2D slides and the topological invariant, like Chern numbers, can only be defined on these 2D slides that do not cross the Weyl points. It is also impossible to directly adopt the evolution of WCs to understand TM because the discussion of WCs has a prerequisite condition: the WCs of WFs must be meaningful. But as discussed by Kivelso et al., the WFs became extended as long as the

---

[*] Electronic address: xiongye@njnu.edu.cn
[†] Electronic address: pqtong@njnu.edu.cn

band gap at the Fermi energy became zero [24–27]. So the traditional WCs of WFs become meaningless in Weyl metals.

In this paper, we adopt the modular operators, e.g. $\hat{x} = \hat{x}_{mod} + \hat{N}_x L$, where $\hat{x}$ is the position operator in the x direction and $\hat{x}_{mod}$ is the modular position operator, which can be expressed as $x_{mod} = x \bmod L$ in the representation of $\hat{x}$ [28]. Here L is the length of a unit cell. We change the definition of WFs, $|\mathrm{WF}\rangle$, from the eigenstates of $\hat{P}\hat{x}\hat{P}$ to those of $\hat{P}\hat{x}_{mod}\hat{P}$, where $\hat{P}$ is the project operator on the occupied states. The WCs of these WFs measured in each unit cell are the eigenvalues of the projected modular position operator. We find that the standard deviation of projected modular position operator, $\langle \mathrm{WF}|\hat{P}\hat{x}^2_{mod}\hat{P}|\mathrm{WF}\rangle$ is zero for every WF $|\mathrm{WF}\rangle$ even when the gap between the occupied bands and the empty bands goes to zero. As a result, the WCs of these newly defined WFs in each unit cell are still meaningful in both TM and TI. By this way, we can universally illustrate the topological properties of TI and TM by evaluating the evolution of WCs.

Although the physical model may be in 2D and 3D, the WFs defined above are 1-dimensional (1D) as they are the eigenstates of the operator $\hat{x}_{mod}$ and the momenta k_y and k_z are only taken as parameters. We find that such WCs of the 1D WFs are equivalent to the phase accumulated by the Bloch states along the Wilson loop in the k_x direction, which has been introduced by Yu et al. and Soluyanov et al. individually [15, 16]. One may regard the extension of the 1D WFs as a new representation of their conclusions, but we should emphasize that beside the application of the 1D WFs to TM, from the present starting point the 2D or higher dimensional WFs can be easily obtained. Previously, such higher dimensional WFs are seldom used in TI due to the reasons such as $[\hat{P}\hat{x}\hat{P}, \hat{P}\hat{y}\hat{P}] \neq 0$ that causes the absence of 2D WFs as common eigenstates of $P\hat{x}\hat{P}$ and $P\hat{y}\hat{P}$. As a contrast, we will show that such obstacle is removed in our consideration because $[\hat{P}\hat{x}_{mod}\hat{P}, \hat{P}\hat{y}_{mod}\hat{P}] = 0$. Here $\hat{y}$ and $\hat{y}_{mod}$ are the position and modular position operators in the y direction, respectively.

This paper is organized as the following: In section II, we show that the states in each band are also the eigenstates of the modular position operators with a certain degenerated eigenvalue x_{mod}. We then show that 3D TI, as well as 3D TM, can be universally illustrated in the same framework with (x_{mod},k_y,k_z). In section III, we extend our WFs from 1D to higher dimensions. We show their applications by illustrating in a plausible way that why the winding numbers $\nu_{2D} = \nu_{3D}$ in two models of the DIII class. In section IV we present the conclusions.

II. 1D MODULAR WANNIER FUNCTIONS IN MULTI-BAND SYSTEMS.

Traditionally, the 1D WFs for the occupied bands are defined as the eigenstates of the projected position operator,

$$\tilde{x} = \hat{P}\hat{x}\hat{P}, \tag{1}$$

where $\hat{x}$ is the position operator in the x direction and $\hat{P} = \sum_{\epsilon_i<0} |\psi_i\rangle\langle\psi_i|$ is the project operator on the occupied states in the Hilbert space. Here, 1D refers to the direction of position operator $\hat{x}$, while the momenta along the other dimensions in the 3D space of the model are taken as parameters. Without loss of generality, we take the Fermi energy as energy zero. These WFs and the corresponding WCs can be denoted as $|x_i\rangle$ and x_i, respectively. The second moment of the WF $l^2 = \langle x_i|(\hat{x} - x_i)^2|x_i\rangle \sim \frac{1}{E_g}$, where E_g is the band gap at the Fermi energy, will diverge as long as $E_g \to 0$. This is why there is no discussion made directly from the point of view of WFs for TMs.

Next we show that this obstacle can be removed when the modular position operator is introduced. We will first introduce the modular variances in a 1D continuum system and then applying them to 1D discrete multi-band models.

For a 1D infinite continuum system in the x direction, one can introduce the modular position operator $\hat{x}_{mod}$ and the modular wave-vector operator $\hat{k}_{mod} = \hat{P}_{mod}/\hbar$ as

$$\hat{x} = \hat{N}_x L + \hat{x}_{mod} \tag{2}$$

$$\hat{k} = \hat{N}_k \frac{2\pi}{L} + \hat{k}_{mod}, \tag{3}$$

where $\hat{P}_{mod}$ is the modular momentum operator in the x direction and $\hat{x}_{mod}$ ($\hat{k}_{mod}$) can only take the eigenvalues in range of $[0, L)$ ($[0, \frac{2\pi}{L})$) in the x (k) representation and $\hat{N}_x$ ($\hat{N}_k$) can only take integer values [28]. Here L is an arbitrary length.

The system can be translated L in the x direction by applying a translation operator $e^{i\hat{k}L} = e^{i\hat{k}_{mod}L}$. Similarly, to translate the system $\frac{2\pi}{L}$ in the momentum space, the translation operator $e^{i\hat{x}\frac{2\pi}{L}} = e^{i\hat{x}_{mod}\frac{2\pi}{L}}$ is needed. It is easy to find that $[e^{i\hat{k}_{mod}L}, e^{i\hat{x}_{mod}\frac{2\pi}{L}}] = 0$. As $e^{i\hat{k}_{mod}L}$ ($e^{i\hat{x}_{mod}\frac{2\pi}{L}}$) is a one-to-one mapping for $\hat{k}_{mod}$ ($\hat{x}_{mod}$), we conclude that $[\hat{x}_{mod}, \hat{k}_{mod}] = 0$ [28]. This means that the modular variances commute although the original variances have $[\hat{x}, \hat{k}] = \frac{i}{2\pi}$.

Such modular variances can be naturally extended to the discrete periodic multi-band models in solid. We take L as the length of a unit cell so that k_{mod} take the value in the FBZ and $G = \frac{2\pi}{L}$ is the reciprocal vector. We denote the ith orbital state in the nth unit cell as $|n\rangle_i$ and the αth band state as $|k\rangle_\alpha$, with $|k\rangle_\alpha = \frac{1}{\sqrt{N}} \sum_{n=1}^{N} e^{iknL} \sum_{j=1}^{m} U_{\alpha j}(k)|n\rangle_j$, where N is the number of the unit cells and $U(k)$ is a unitary matrix. There are totally m orbital states in each unit cell so that there are m bands in the FBZ. The wave-vector operator $\hat{k}$ and the position operator $\hat{x}$ are defined in the real space by

$$e^{i\hat{k}L}|n\rangle_i = |n-1\rangle_i \tag{4}$$
$$\hat{x}|n\rangle_i = (nL + X_i)|n\rangle_i, \tag{5}$$

where $X_i \in [0, L)$. As $e^{i\hat{k}L} = e^{i\hat{k}_{mod}L}$ and $e^{i\hat{x}G} = e^{i\hat{x}_{mod}G}$, in the reciprocal space, by applying the above equations to $|k\rangle_\alpha$, we have

$$e^{i\hat{k}_{mod}L}|k\rangle_\alpha = e^{ikL}|k\rangle_\alpha \tag{6}$$
$$e^{i\hat{x}_{mod}G}|k\rangle_\alpha = e^{i\theta_\alpha}|k\rangle_\alpha. \tag{7}$$

In the last equation, we have used the property that in the reciprocal space, the states $|k\rangle_\alpha$ and $|k+G\rangle_\alpha$ must represent the same quantum state with only a possible phase difference $\theta_\alpha \in [0, 2\pi)$. Here θ_α is independent of k because these transformations for different $|k\rangle$ will map to the same Wilson loop with only starting point difference. Like that in the continuum model, $[e^{i\hat{k}_{mod}L}, e^{i\hat{x}_{mod}G}] = 0$ so that $\hat{k}_{mod}$ and $\hat{x}_{mod}$ are diagonalized simultaneously in the reciprocal space for each band. These N-fold degenerated eigenvalues of $\hat{x}_{mod}$ for each band correspond to N WFs with their WCs at $x_{mod} = \theta_\alpha/G$ in each unit cell.

As $\hat{x}_{mod}$ is diagonal for each band, one can apply the occupied project operator $\hat{P}$ from the left and the right sides straightforwardly and the second moment of the eigenstates of the projected modular position operator, $\langle x_i|\hat{P}\hat{x}^2_{mod}\hat{P}|x_i\rangle - \langle x_i|\hat{P}\hat{x}_{mod}\hat{P}|x_i\rangle^2$ is fixed at zero. We want to emphasize that in the above derivations, we only suppose that each band is either fully occupied or empty but do not require a finite band gap at the Fermi energy.

In the case of multi-bands being occupied, it will be hard to distinguish the band index α in the presence of band crossing. This difficulty can be overridden by studying the matrix $\hat{P}e^{i\hat{x}_{mod}G}\hat{P}$. This operator represents how much phase is accumulated for the states $|k\rangle_\alpha$ by mapping to $|k+G\rangle_\alpha = |k\rangle_\alpha$. One can divide this mapping into N_k segments, $F_{n_k} = \hat{P}e^{i\hat{x}_{mod}G/N_k}\hat{P}$ with $n_k \in (1, 2, \cdots, N_k)$. Then the phases $\hat{x}_{mod}G$ can be obtained by finding the phases of the eigenstates of the product matrix $\Pi_{n_k=1}^{N_k} F_{n_k}$. The above mapping is equivalent to the product of the non-abelian Berry connection along the "Wilson loop" raised in Ref. [15, 16]. And the phases $x_{mod}G = \theta_\alpha$ are equal to the phases denoted by θ^D_m in Ref. [16].

Now we apply the above results to a 3D Weyl metal with the effective Hamiltonian

$$\begin{aligned} H_W &= [M_0 + \beta_1(\cos(k_x) + \cos(k_y)) + \beta_2\cos(k_z)]\sigma_z \\ &\quad + \sin(k_x)\sigma_x + \sin(k_y)\sigma_y, \end{aligned} \tag{8}$$

where $\sigma_{x(yz)}$ is the Pauli matrix along $x(yz)$ direction. Here we fix $\beta_1 = 0.2$ and $\beta_2 = 0.4$.

The model has two Weyl points at $(k_x, k_y, k_z) = (0, 0, \pm 1.29)$ when $M_0 = -0.5$. Like the applications in 3D TI [17], we can take the two wave-vectors, e.g. k_x and k_z, as parameters and find the eigenvalues of $\hat{P}\hat{y}_{mod}\hat{P} = \theta_y/G$ along the rest y direction. In Fig. 1, we plot the function $\theta_y(k_x, k_z)$ in the range $[-\pi, \pi]$. θ_y is 2π folded along the line connecting the two Weyl points (projected on the $k_x - k_z$ plane) which is the projection of the Dirac string on the $k_x - k_z$ plane. Imagine that we are varying the wave-vectors along the typical paths C_1 and C_2 shown in Fig. 1. The WCs of WFs will come back to their original positions when the varying is along C_1. But the WCs change one unit cell when the varying is along C_2. By applying Laughlin's cylinder argument, we can conclude immediately that there should be boundary states that cross the zero energy on the xz surface to compensate the movements of WFs to make the situation totally unchanged when the wave-vector comes back along C_2 on the 2D FBZ torus. But such zero energy surface state does not exist when the varying is along C_1. So these zero energy boundary states form the unclosed Fermi arc on the $x - z$ surface of the 3D Weyl metal.

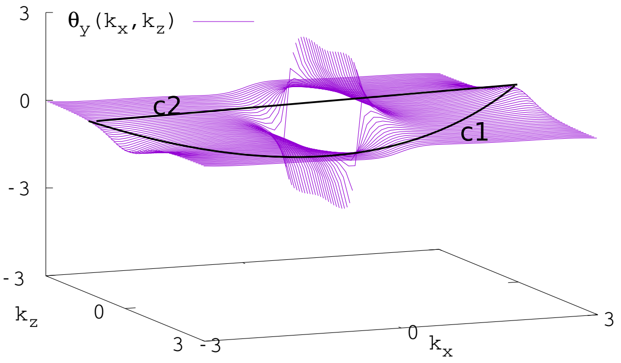

FIG. 1: θ_y as a function of k_x and k_z. θ_y acquires a 2π (0) variation when (k_x, k_z) evolves along c_2 (c_1). Here $N_k = 20$.

We find a similar plot for $\theta_x(k_y, k_z)$, which indicates that Fermi arc can also appear at the $y - z$ surface. But we find a trivial $\theta_z(k_x, k_y)$, keeping at 0 for any k_x and k_y, which indicates that there is no Fermi arc at the xy surface of the Weyl metal.

The model can have 6 Weyl points at $(0, \pi, \pm 0.73)$, $(\pi, 0, \pm 0.73)$ and $(0, 0, \pm 1.82)$ when $M_0 = -0.3$. We plot the function $\theta_y(k_x, k_z)$ in Fig. 2. As that in Fig. 1, the plot illustrates the topological properties of the Weyl metal explicitly. The evolution of $\theta_x(k_y, k_z)$ is also similar to $\theta_y(k_x, k_z)$ and $\theta_z(k_x, k_y)$ is trivial as well.

By the two illustrative models, we show the power of the WFs defined by modular position operator. For the first time, we can understand TM by considering the 3D FBZ as a whole, otherwise one usually needs to employ a series of 2D planes or 2D cylinders in the FBZ to discuss

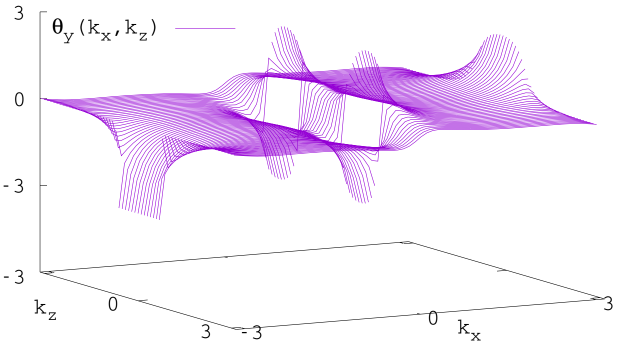

FIG. 2: θ_y as a function of k_x and k_z for the model with totally 6 Weyl points.

topological properties of TM.

III. EXTENDED WANNIER FUNCTIONS TO HIGHER DIMENSIONS

In this section, we show that with the help of the modular position operators, we can easily find WFs in higher dimensions. We will show the application of 2D WFs in two 3D illustrative lattice models in the DIII class.

By applying Eq. 7, we have

$$e^{i\hat{x}_{mod}G_x}|k_x,k_y\rangle_\alpha = e^{i\theta^x_\alpha(k_y)}|k_x,k_y\rangle_\alpha \tag{9}$$

$$e^{i\hat{y}_{mod}G_y}|k_x,k_y\rangle_\alpha = e^{i\theta^y_\alpha(k_x)}|k_x,k_y\rangle_\alpha, \tag{10}$$

where $|k_x,k_y\rangle_\alpha$ denotes the eigenstate in the αth band with momenta k_x and k_y in the 2D FBZ. Here, $\theta^{x(y)}_\alpha(k_{y(x)})$ is a function of $k_{y(x)}$ so that x_{mod} and y_{mod} (the eigenvalues of the modular operators) are not uniform in each unit cell. This is the key difference between WFs in higher dimensions and those in 1D.

As the modular position operators, $\hat{x}_{mod}$ and $\hat{y}_{mod}$, are diagonal for each band, we have $[\hat{P}\hat{x}_{mod}\hat{P},\hat{P}\hat{y}_{mod}\hat{P}]=0$. But for the position operators, one has $[\hat{P}\hat{x}\hat{P},\hat{P}\hat{y}\hat{P}]\neq 0$ [26]. This is why after defining the WFs by the modular position operators, we can extend WFs to higher dimensions easily.

We next show how to find the WCs of the WFs in 2D. The method is straightforwardly to be applied in further higher dimensions. We take a square 2D FBZ as an instance. We discretize the FBZ into N^2 elements by N rows and N columns and denote the state in each cell as $|n_x,n_y\rangle_\alpha = |-\frac{G_x}{2}+n_x\delta k_x,-\frac{G_y}{2}+n_y\delta k_y\rangle_\alpha$, where $G_{x(y)}$ is the reciprocal vector and $\delta k_{x(y)} = G_{x(y)}/N$. We calculate the operators

$$XY^+ = \hat{P}e^{i(\hat{x}\delta k_x+\hat{y}\delta k_y)}\hat{P} \tag{11}$$

$$XY^- = \hat{P}e^{i(\hat{x}\delta k_x-\hat{y}\delta k_y)}\hat{P}, \tag{12}$$

in the discrete FBZ. Most elements of $XY^\pm$ are zero except $XY^+_{n_x,n_y;n_x+1,n_y+1}$ for XY^+ and $XY^-_{n_x,n_y;n_x+1,n_y-1}$ for XY^-. Furthermore, $XY^\pm$ can be block diagonalized into N independent $N\times N$ matrix, with each matrix mimics the $\hat{X}_P(k_y)$ matrix in Eq. 6 in Ref. [16],

$$XY^\pm(n) = \begin{pmatrix} 0 & XY^\pm_{1,n;2,n\pm1} & 0 & \cdots \\ 0 & 0 & XY^\pm_{2,n\pm1;3,n\pm2} & \cdots \\ \cdots & \cdots & \cdots & \cdots \\ XY^\pm_{N,n\pm N;1,n} & 0 & 0 & \cdots \end{pmatrix}. \tag{13}$$

The phases of the eigenvalues of the product matrix $XY^\pm_{1,n;2,n\pm1}XY^\pm_{2,n\pm1;3,n\pm2}\cdots XY^\pm_{N,n\pm N;1,n}$ give the N-fold degenerated values $x_{mod}G_x \pm y_{mod}G_y$ (mod 2π). Like the 1D case, these N-fold degenerated modular positions correspond to WCs localized at different unit cells. But as there are N independent $XY^\pm(n)$, we will have totally N kinds of N-fold degenerated values $x_{mod}G_x \pm y_{mod}G_y$ (mod 2π). So we can conclude that the 2D WCs defined by these modular position operators are not uniform in each unit cell in the 2D lattice. This is consistent with the previous argument that the 2D WFs with uniform WCs do not exist in 2D topological nontrivial lattice [25].

Now we apply the above method to find 2D WFs for two 3D lattice models. We will take the momentum, e.g. k_x, as a parameter and study how the 2D WCs evolve as k_x is varying 2π in the FBZ. Such illustration provides more information than the evolution of 1D WCs as varying, e.g. both k_x and k_y.

We start from a 3D illustrative model in the DIII class,

$$H(\vec{k}) = \begin{pmatrix} \epsilon(\vec{k})I & \Theta(\vec{k}) \\ \Theta^\dagger(\vec{k}) & \epsilon(\vec{k})I \end{pmatrix}, \tag{14}$$

with $\Theta(\vec{k}) = i(\vec{d}\cdot\vec{\sigma})\sigma_y$, where the unit matrix I and Pauli matrix $\vec{\sigma} = (\sigma_x,\sigma_y,\sigma_z)$ are all 2×2 matrix [29].

As in Ref. [29], we denote the Hamiltonian as H_1 when $\epsilon(\vec{k}) = \cos(k_x-k_z)+\cos(k_x)+2\cos(k_y-k_z)+\cos(k_y)-\mu$ and $(d_x,d_y,d_z) = \Delta([\sin(k_x-k_z)+\sin(k_x)+2\sin(k_y-k_z)-\sin(k_y)],2\sin(k_y),2\sin(k_x+k_y))$. The winding number ν_{3D} for this model can take nontrivial value ±1 [29]. Here we take $\Delta = 5$ and $\mu = 2.5$ so that $\nu_{3D} = 1$ in our calculation. Finch et. al argued in Ref. [29] that when a breaking symmetry term is added to the Hamiltonian on the surface of this TI, e.g. on the xy surface, to open up a gap for the surface states, one is able to obtain the winding number for the gapped surface states, ν_{2D}, and found that $\nu_{3D} = \nu_{2D}$.

In Fig. 3 (a) and (b), we illustrate how $\theta^\pm_{yz}(n) = G(y_{mod}\pm z_{mod})$ evolve with k_x, where $G = G_x = G_y = \frac{2\pi}{a}$ is the reciprocal vector and $y_{mod}(z_{mod})$ is the eigenvalues of the modular position operators $\hat{y}_{mod}(\hat{z}_{mod})$. Here, for the sake of clarity, we divide the whole FBZ into 4×4 blocks so that there are 4 kinds of $\theta^\pm_{yz}(n)$, which are identified by the index $n = 0,1,2,3$ in the figure. Dividing the FBZ into smaller parts will not alter the key features of the figures. As the figure shows, most of the modular positions experience a trivial evolution with k_x. But there is one modular position (one for $y_{mod}+z_{mod}$ and one for $y_{mod}-z_{mod}$ respectively) that undergoes a change of unit cell a as varying a reciprocal vector for k_x.

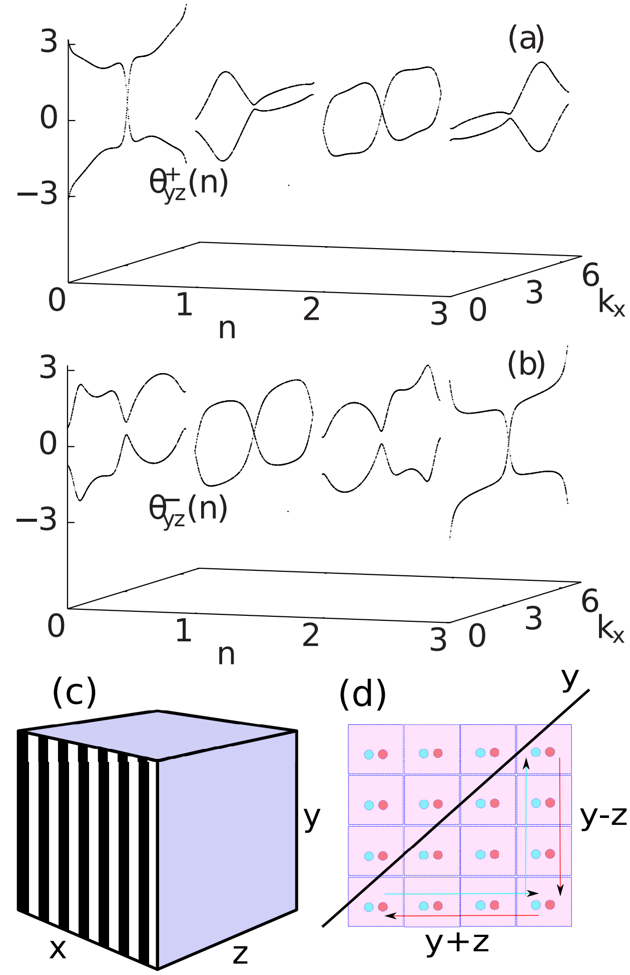

FIG. 3: $\theta^{\pm}_{yz}=G(y_{mod}\pm z_{mod})$ as functions of k_x in (a) and (b). The 2D FBZ in k_y and k_z plane is divided in to 4×4 blocks. $n=0,1,2,3$ are the 4 kinds of $\theta^{\pm}_{yz}$. Here the lattice constant a is taking as the unit. (c) shows the 3D topological insulator with breaking symmetry term added on the xy surface. We show how the WCs of WFs evolve with k_x in the 2D real space in (d), with red and green dots representing the two WCs in each unit cell. The arrows indicate the variations of WCs by changing k_x from 0 to $2\pi/a$. Most of them undergo a trivial evolution except those along a column and a row.

Such behavior of evolution reflects the bulk topological properties of the 3D model which can not be modified by adding a symmetry breaking term on the xy surface. We explicitly illustrate how these WCs evolves with k_x in the 2D real plane yz in Fig. 3 (d). Points in each unit cell are representing the WCs of the WFs. The exact order of columns or rows are not important because a gauge transformation can exchange them. This figure shows that there is one WF that being pumped one half lattice constant from left to right (and another WF that is pumped one half lattice constant inversely) along y axis as varying k_x circularly from 0 to $2\pi/a$. To compensate such evolution for the gauge invariant, there should be topological protected edge states at the edge of either gapped or gapless xy surface. Because of the bulk-boundary correspondence for TI, each xy surface should contribute 1/2 winding, which takes the responsibility of the half lattice movement of the WFs during the k_x pump. As a result, ν_{2D}, which counts the total winding of the two xy surfaces, is totally 1. This is what $\nu_{3D}=\nu_{2D}$ means for this model.

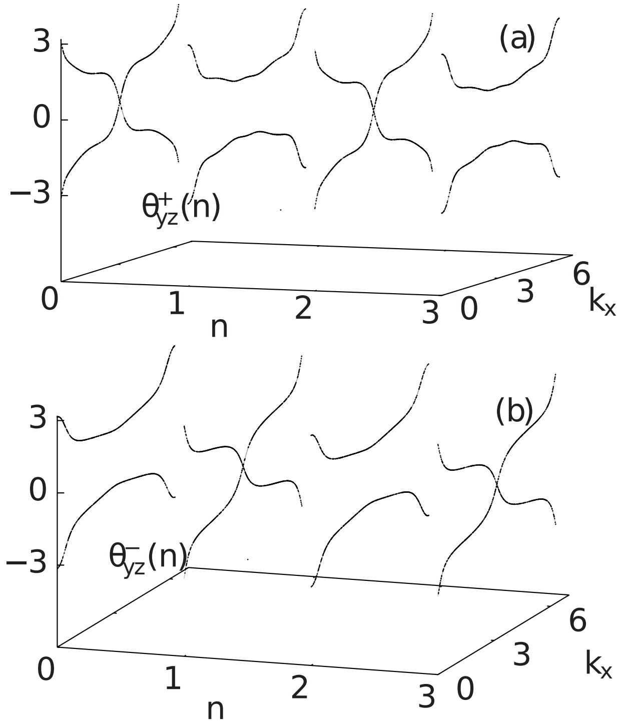

FIG. 4: $\theta^{\pm}_{yz}=G(y_{mod}+z_{mod})$ as functions of k_x in (a) and (b). The 2D FBZ in k_y and k_z plane is divided in to 4×4 blocks. $n=0,1,2,3$ are the 4 kinds of $\theta^{\pm}_{yz}$.

We then do a similar discussion on another model H_2 with $\epsilon(\vec{k})=\cos(k_x)+\cos(k_x-k_z)-\mu$ and $(d_x,d_y,d_z)=\Delta(\sin(k_x)+\sin(k_x-k_z),2\sin(k_y),2\sin(k_x-k_z))$. We take $\Delta=2$ and $\mu=1$ in the calculation. The model is in the topological phase with $\nu_{3D}=2$.

In Fig. 4, we show how $G(y_{mod}+z_{mod})$ and $G(y_{mod}-z_{mod})$ evolve with k_x. There are two modular positions experience nontrivial evolution along $y+z$ or $y-z$ direction. This makes us infer that there are two WCs being pumped half a unit cell from left to right and another two WCs vice versa. Applying the similar discussion as we have done for the previous model we can conclude that $\nu_{2D}=2$. This also matches the equation $\nu_{3D}=\nu_{2D}$ for this model.

We have also applied similar calculations for H_3 and H_4 in the topological phase with $\nu_{3D}=3$ and $\nu_{3D}=4$ [29]. But we find that the evolution of 2D WCs are not simply extended as that from H_1 to H_2. Typically for H_4, we find the evolution of 2D WCs are *all trivial*. One possible explanation is that the evolution of 2D WFs can not universally represent all TIs of the DIII class. But we propose that it is because another factor which has not been discussed in Ref. [29], the disorder effect. Our discussion is based on a gauge argument. So the conclusion naturally possesses the effect of disorder even though the disorder term is not explicitly engaged. For H_4 with $\nu_{3D} = 4$, there is two pair of chiral edge states at the boundary of the 2D xy surface. Although the symmetry may still prevent the intra-pairing back scattering, it can not prevent the inter-pairing back scattering in the presence of disorder. So the disorder can smear out the edge states near the zero energy and open up an effective gap. This is why we find the trivial 2D WCs evolution for H_4 and it will need further numerically investigation to be proved.

IV. CONCLUSIONS

We modify the definition of WFs for the occupied bands by introducing the modular position operators. One can calculate these 1D WFs along the Wilson loop along one direction of the FBZ. The topological nontrivial band structure can be illustrated by the nontrivial evolution of WCs as varying the momentum in the other directions. We show that such illustration, usually only applied to TI, can also be applied to Weyl metal in which there is no band gap at the Fermi surface. Our illustration well explains the nontrivial band structure of Weyl metal as well as the Fermi arc for the surface states. We also extend the 1D WFs to higher dimensions. We show its application on explaining $\nu_{3D} = \nu_{2D}$ in the two models belonging to the DIII class.

Acknowledgments.— The work was supported by the State Key Program for Basic Research of China (Grant Nos. 2009CB929504, 2009CB929501), National Foundation of Natural Science in China Grant Nos. 10704040, 11175087.

---

[1] K. v. Klitzing, G. Dorda, and M. Pepper, Phys. Rev. Lett. **45**, 494 (1980), URL `http://link.aps.org/doi/10.1103/PhysRevLett.45.494`.

[2] D. J. Thouless, M. Kohmoto, M. P. Nightingale, and M. den Nijs, Phys. Rev. Lett. **49**, 405 (1982), URL `http://link.aps.org/doi/10.1103/PhysRevLett.49.405`.

[3] J. E. Avron, R. Seiler, and B. Simon, Phys. Rev. Lett. **51**, 51 (1983), URL `http://link.aps.org/doi/10.1103/PhysRevLett.51.51`.

[4] B. Simon, Phys. Rev. Lett. **51**, 2167 (1983), URL `http://link.aps.org/doi/10.1103/PhysRevLett.51.2167`.

[5] M. Kohmoto, unpublished.

[6] R. B. Laughlin, Phys. Rev. B **23**, 5632 (1981), URL `http://link.aps.org/doi/10.1103/PhysRevB.23.5632`.

[7] L. Fu and C. L. Kane, Phys. Rev. B **74**, 195312 (2006).

[8] B. A. Bernevig, T. L. Hughes, and S.-C. Zhang, Science **314**, 1757 (2006), http://www.sciencemag.org/content/314/5806/1757.full.pdf.

[9] M. Z. Hasan and C. L. Kane, Rev. Mod. Phys. **82**, 3045 (2010).

[10] S.-Q. Shen, *Topological Insulators, Dirac Equation in Condensed Matters* (Springer Series in Solid-State Science 174, 2012).

[11] G. E. Volovik, *The Universe in a Helium Droplet* (Clarendon Press, Oxford, 2003).

[12] A. P. Schnyder, S. Ryu, A. Furusaki, and A. W. W. Ludwig, Phys. Rev. B **78**, 195125 (2008).

[13] C. Nayak, S. H. Simon, A. Stern, M. Freedman, and S. Das Sarma, Rev. Mod. Phys. **80**, 1083 (2008).

[14] X.-L. Qi and S.-C. Zhang, Rev. Mod. Phys. **83**, 1057 (2011).

[15] A. A. Soluyanov and D. Vanderbilt, Phys. Rev. B **83**, 235401 (2011), URL `http://link.aps.org/doi/10.1103/PhysRevB.83.235401`.

[16] R. Yu, X. L. Qi, A. Bernevig, Z. Fang, and X. Dai, Phys. Rev. B **84**, 075119 (2011), URL `http://link.aps.org/doi/10.1103/PhysRevB.84.075119`.

[17] M. Taherinejad, K. F. Garrity, and D. Vanderbilt, Phys. Rev. B **89**, 115102 (2014), URL `http://link.aps.org/doi/10.1103/PhysRevB.89.115102`.

[18] X.-L. Qi, Phys. Rev. Lett. **107**, 126803 (2011), URL `http://link.aps.org/doi/10.1103/PhysRevLett.107.126803`.

[19] Y.-L. Wu, N. Regnault, and B. A. Bernevig, Phys. Rev. B **86**, 085129 (2012), URL `http://link.aps.org/doi/10.1103/PhysRevB.86.085129`.

[20] M. Taherinejad and D. Vanderbilt, Phys. Rev. Lett. **114**, 096401 (2015), URL `http://link.aps.org/doi/10.1103/PhysRevLett.114.096401`.

[21] H. Search, C. Journals, A. Contact, M. Iopscience, N. J. Phys, and I. P. Address, New Journal of Physics **9**, 356 (2007), ISSN 1367-2630, URL `http://stacks.iop.org/1367-2630/9/i=9/a=356?key=crossref.45`

[22] X. Wan, A. M. Turner, A. Vishwanath, and S. Y. Savrasov, Phys. Rev. B **83**, 205101 (2011), URL `http://link.aps.org/doi/10.1103/PhysRevB.83.205101`.

[23] A. A. Burkov and L. Balents, Phys. Rev. Lett. **107**, 127205 (2011), URL `http://link.aps.org/doi/10.1103/PhysRevLett.107.127205`.

[24] S. Kivelson, Phys. Rev. B **26**, 4269 (1982).

[25] D. Thouless, J. Phys. C **17**, L325 (1984).

[26] N. Marzari and D. Vanderbilt, Phys. Rev. B **56**, 12847 (1997), URL `http://link.aps.org/doi/10.1103/PhysRevB.56.12847`.

[27] T. Thonhauser and D. Vanderbilt, Phys. Rev. B **74**, 235111 (2006).

[28] Y. Aharonov and D. Rohrlich, *Quantum Paradoxes* (WILEY-VCH Verlag GmbH Co. KGaA, 2005).

[29] P. Finch, J. de Lisle, G. Palumbo, and J. K. Pachos, Phys. Rev. Lett. **114**, 016801 (2015), URL `http://link.aps.org/doi/10.1103/PhysRevLett.114.016801`.